Research paper

The use of inorganic Al-HMS as a support for NiMoW sulfide HDS catalysts

R. Huirache–Acuña [a],[*], T.A. Zepeda [b], P.J. Vázquez [a], E.M. Rivera-Muñoz [c], R. Maya-Yescas [a], B. Pawelec [d], G. Alonso-Núñez [b]

[a] *Facultad de Ingeniería Química, Universidad Michoacana de San Nicolás de Hidalgo, 58060 Morelia, Michoacán, Mexico*
[b] *Centro de Nanociencias y Nanotecnología – UNAM, 22800 Ensenada, B.C., Mexico*
[c] *Centro de Física Aplicada y Tecnología Avanzada-UNAM, 76230 Juriquilla, Querétaro, Mexico*
[d] *Instituto de Catálisis y Petroleoquímica, CSIC, c/Marie Curie 2, Cantoblanco, Madrid 28049, Spain*

ARTICLE INFO

ABSTRACT

Inorganic hexagonal mesoporous silica (HMS) and aluminum modified HMS materials (Al-HMS) were prepared and used as supports of transition metal sulfide hydrodesulfurization (HDS) catalysts based on nickel, molybdenum, and tungsten as active phase. The samples were characterized with XRD, HRTEM, TPD, N_2 physisorption and UV–Vis. The catalytic activity of the trimetallic catalysts was performed in the HDS of dibenzothiophene (DBT). When Al was incorporated into the inorganic support, important changes and effects were observed on the physicochemical properties. On the other hand, the incorporation of Al into the HMS led to a decrease in the reaction rate (k) and a trend toward a direct path of desulfurization was observed for all materials.

1. Introduction

Currently, research projects for the development of more effective HDS catalysts have become an important topic of study for environmental catalysts around the world [1–4]. Environmental regulations in many countries require the production of transport fuels with lower sulfur contents (less than 10 ppm) [1–4].

Over the past 20 years has been a global trend to reduce levels of sulfur compounds in fossil fuels because they are precursors of sulfur oxide and in addition to poison the transition metals present in other stages of refinement. Among the sulfur compounds in petroleum fractions include thiols, sulfides, disulfides, thiophenes, benzothiophenes, and dibenzothiophenes compounds. The ability to remove the sulfur content in the organic molecules depends on the molecule complexity (molecular size and structure of organo-soaked compounds) [5]. The complexity of sulfur removal increases in the following order: thiophenes > benzothiophenes > dibenzothiophenes. In recent years, for deep HDS processes, it is explored and investigated the design of new catalysts based on the synthesis and application of inorganic molecular sieves based on mesoporous silica as catalyst supports [6–8]. The design procedure makes use of the high surface areas that exhibit this type of materials to achieve higher activity per unit weight. At the same time, the uniform mesoporous structure facilitates the dissemination of the polycyclic compounds of sulfur and the surface acidity contributes the metals' dispersion.

Pure or modified inorganic mesoporous silica-based materials with heteroatoms such as Ti, Al, Zr or Nb [9–22], have attracted considerable attention as possible supports for the preparation of hydroprocessing catalysts. These features of HMS supports have enabled the preparation of transition metal sulfided CoMo and NiMo bimetallic catalysts with higher catalytic activity in comparison with a CoMo/Al_2O_3 commercial catalyst in the HDS reaction of DBT [6,13,18], and even better than other inorganic materials such as SBA-15 or MCM-41 [23]. Regarding the active phase generally, bimetallic formulations have been used [24–26]. However, in 2001, Soled *et al.* patented a novel unsupported trimetallic catalyst called NEBULA (New Bulk Activity) based on transition metals, which presents the highest catalytic activity for HDS reactions [27]. Subsequently, R. Huirache-Acuña and co-workers [28]

* Corresponding author.
  E-mail address: rafael_huirache@yahoo.it (R. Huirache–Acuña).

reported the synthesis of a trimetallic-type catalyst mass (unsupported) with high catalytic activity in the HDS of DBT. However mass type catalysts have a higher cost compared to typical supported catalytic materials. Therefore, it is very important to investigate the use of tri-metallic transition metal sulfide as active phases of catalysts supported on inorganic supports. Nowadays, to lowering the catalyst cost, one of the procedures for deep desulfurization on which this research proposal is based, is to increase the catalytic activity by obtaining more effective hydrodesulfurization catalysts. For this reason, it is of great importance the search of inorganic HMS and Al-HMS supports for the preparation of novel trimetallic catalysts, which favors the formation of active sites for the HDS reaction, in addition to reducing the catalyst cost.

2. Experimental

2.1. Synthesis of inorganic HMS and Al-HMS

Inorganic Hexagonal Mesoporous Silica materials (HMS) and Al-HMS (Si/Al = 60, 40 and 20) were prepared by the method of sol–gel [29]. A summary of this procedure is described below: first, a homogeneous solution of dodecylamine surfactant (DDA, 98% Aldrich, 4.7554 g or 5.9 mL), was dissolved in ethanol (58.4 mL, Sigma-Aldrich) and the right quantity of deionized water was added under constant stirring (H_2O, 234.2 mL); then, mesitylene (MES, 97% Aldrich, 16.1 mL) was added to the above solution with stirring at room temperature for 20 min. Subsequently, a solution of tetraethylorthosilicate (TEOS, 98%, 22.8 mL, Aldrich) was slowly added and allowed to perform the reaction (hydrolysis and condensation) with stirring at room temperature for 20 h. Finally, the solid obtained was recovered by filtration, washed with deionized water and dried at room temperature, followed by drying at 110 °C. The organic material is removed by calcination in air at 550 °C for 4 h. The molar ratios of the reagents used are 1 mol TEOS: 0.25 mol DDA: 10 mol Ethanol: 130 mol H_2O: 1.125 mol MES. Mesoporous silica containing aluminum (Al-HMS) was also synthesized using the same procedure as for the material of HMS, but this time by dissolving the appropriate amount of aluminum (AlPO, 97%, Aldrich) in TEOS in order to obtain samples with Si/Al molar ratios of 20, 40 and 60.

2.2. Trimetallic transition metal catalysts synthesis

All NiMoW/HMS and NiMoW/Al-HMS catalysts were prepared by simultaneous support impregnation with metal oxide precursors via incipient wetness method. In a typical synthesis, precursors salts were dissolved in deionized water: $(NH_4)_6Mo_7O_{24}\cdot6H_2O$ (AHM, ammonium heptamolybdate)), $(NH_4)_6H_2W_{12}O_{40}\cdot xH_2O$ (AMT, ammonium metatungstate)), and $Ni(NO_3)_2\cdot6H_2O$ (nickel nitrate hexahydrate) were employed as the precursors of MoO_3, WO_3 and NiO, respectively. The supports were loaded with fixed amounts of molybdenum (8.53 wt%), tungsten (13.75 wt%) and nickel (3.81 wt%). The concentrations were calculated to achieve a Mo/W atomic ratio of 0.5 and a Ni/Mo atomic ratio of 0.3.

The solution of AHM was poured into the solution of AMT with constant stirring, and then the solution of nickel nitrate hexahydrate was added into the mixture. The solution was added dropwise using constant stirring until the homogeneous humidification of the support was completed. Then, it was immediately subjected to drying in a furnace at 85 °C for 16 h, and calcined at 500 °C for 4 h, in both treatments using a temperature profile of 2 °C/min.

2.3. Materials characterization

Determination of the surface area (S_{BET}) was performed by N_2 Physisorption at −196 °C using a Micromeritics TriStar 3000 apparatus, having each sample a pretreatment to remove any organic component and humidity (degassing) of 5 h at 270 °C in an inert atmosphere. In order to avoid the tensile strength (TSE) artifact, pore size distribution (PSD) curves were calculated by applying the Barret-Joyner-Halenda method (BJH) to the adsorption branches of the N_2 isotherms. The total pore volume (Vt) was obtained from the isotherms at $P/P_0 = 0.99$.

The identification of the crystalline phases of the catalysts in the form of oxides and sulfides were characterized by X-ray diffraction by the powder method with a computerized Seifert 3000 diffractometer, using Ni-filtered Cu Kα ($\lambda = 0.1541$ nm) radiation, a PW 2200 Bragg-Brentano $\theta/2\theta$ goniometer equipped with a bent graphite monochromator and an automatic slit, and a step size of 0.01°.

The acidity of the materials was determined by desorption of ammonia at programmed temperature (TPD of NH_3) carried out in a Micromeritics TPR/TPD 2900 with a thermal conductivity detector (TCD). Samples (0.050 g) were degassed in a He (99.996%) flow at 250° C for 1 h. Then, the sample was cooled to a temperature of 100° C and saturated with a stream of NH_3 (5% NH_3/He) at a flow rate of 50 mL/min for 1 h, followed by He flow for 15 min. Desorption was carried out by heating the sample up to 700° C with a heating rate of 15 °C / min. To determine the total acidity based on its NH_3 desorption profile, the area under the curve was integrated. Weak, medium and strong acidities were defined as the area under the curve of the peaks in the temperature ranges of 100–250 °C, 250–400 °C, and 400–600 °C, respectively.

The diffuse reflectance spectra were obtained using a UV–vis spectrophotometer Varian Cary by 5000. The acquisition range of 200–900 nm was at room temperature with a recording speed of 120 nm/min.

The study by transmission electron microscopy (TEM) was performed to the sulfided catalysts. A JEOL 100 CXII microscope operating at a 200 kV voltage and equipped with an X-ray signal INCA (Oxford Instruments) was used. The sample was dispersed in ethanol with an ultrasonic bath at room temperature. Finally, a drop of the suspension was placed on a copper grid coated with carbon. Statistical evaluation of about 50 particles was performed from various TEM images.

2.4. HDS performance (catalytic activity)

The HDS of DBT reaction was performed in a batch reactor (Parr model 4848 high-pressure). First, sulfurization of the catalysts was performed in a fixed bed reactor made of borosilicate glass with a gas mixture of 15%H_2S/85%H_2 (Praxair) at a flow of 60 mL min^{-1}, raising the temperature at a rate of 10 °C to 400 °C min^{-1}, where the samples stayed for 2 h. Then, the samples were cooled down to room temperature under a nitrogen flow and were placed in a beaker with hexadecane to prevent oxidation of the activated catalyst. The transition metal sulfide catalysts were then introduced into the reactor. The reactor was heated at a rate of 5.5 °C min^{-1} up to 320 °C and pressurized by using hydrogen to 5.4 MPa. Regarding the stirring speed, this remained intensive (700 rpm) to prevent external diffusion constraints. The reaction time comprises 270 min and sampling for chromatographic analysis was conducted in the following periods: 0, 15, 30, 45, 60, 90, 120, 150, 210 and 270 min. Analyses of the samples were performed during the course of each run to determine the conversion against time dependence. Each reaction required 500 ppm of sulfur (about 0.226 g of DBT), 100 mL of hexadecane as solvent and 0.255 g of each catalyst. The course of each reaction was followed by taking liquid samples at the times aforementioned and analyzing then in a gas chromatograph Agilent Technologies 7890A GC System Model which features a 30 m HP5 column with capillary length and an internal diameter of 0.32 mm, equipped with a detector type Agilent 355 SCD. The products obtained after the conversion of the DBT were biphenyl (BP) as direct desulfurization (DDS) product, while bicyclohexyl (BCH), cyclohexylbenzene (CHB) and traces of tetrahydrodibenzothiophene (THDBT) were the products resulting from the hydrogenation pathway (HYD). Direct desulfurization (DDS) and hydrogenation (HYD) selectivity were defined as:

(DDS): (BP) × 100% /(CHB + BP + BCH + THDBT)

(HYD): (CHB + BCH + THDBT) × 100% / (CHB + BP + BCH + THDBT)

HDS kinetic constants (k) were calculated assuming pseudo-first

order kinetics referred to initial DBT concentration.

$$k \cdot t = - \ ln(1-x) \tag{1}$$

where t is reaction time, and x is the conversion of DBT. Catalytic tests were performed varying the particle size and stirring rate to found an experimental error value between 3.5 and 5.4%.

3. Results and discussion

3.1. Characterization of oxide catalyst precursors

3.1.1. Textural properties of synthesized materials

The textural properties of the HMS-Al (40) pure support and calcined NiMoW/HMS-Al(40) catalyst precursors were studied by N_2 physisorption at −196 °C (Fig. 1).

As expected, a large decrease in the amount of adsorbed nitrogen is observed after the incorporation of a large amount of metal oxides. The N_2 isotherms of NiMoW/HMS-Al(40) catalyst have two capillary condensation steps: (i) the first hysteresis loop for these materials starts at a partial pressure of about 0.40, indicating the presence of framework mesoporosity and (ii) the second hysteresis loop starting at a relative pressure of about 0.88 might to be attributed to either to macropores or to textural interparticle mesoporosity, which takes place when the particle diameters are very small and closely packed [30].

The N_2 adsorption–desorption isotherms corresponding to transition metal NiMoW catalysts supported on inorganic HMS and Al-modified HMS material (varying the Si/Al = 20, 40, 60) are presented in Fig. 2. It is observed that all materials exhibit type IV isotherms (IUPAC classification), which is associated with mesoporosity and show "bottle-neck" hysteresis [31], mainly in catalysts with Si/Al = 60 ratio and for pure HMS.

The S_{BET} values of the catalysts in their oxide state are shown in Table 1. It was observed that when the aluminum concentration increases (Si/Al = 20 > Si/Al = 40 > Si/Al = 60) it leads to a decrease in the S_{BET} values in all cases, probably due to a progressive blockage of the supports pores by the metal particles formed during impregnation-calcination process. However, this behavior was not lineal since the support with a higher amount of aluminum (Si/Al = 20) shows a S_{BET} value of 483 m²/g, which is higher compared with that observed for the

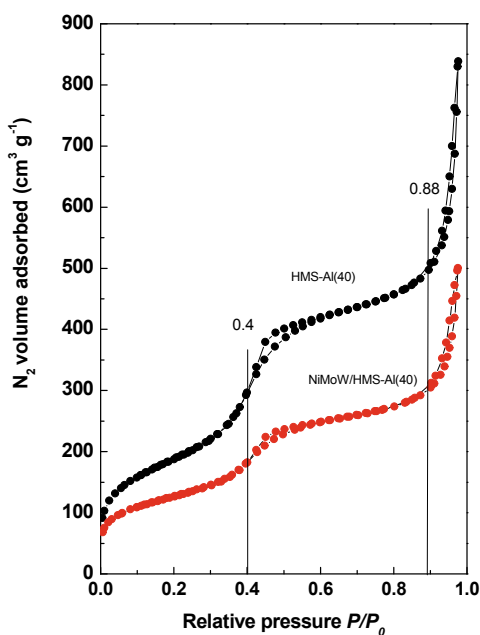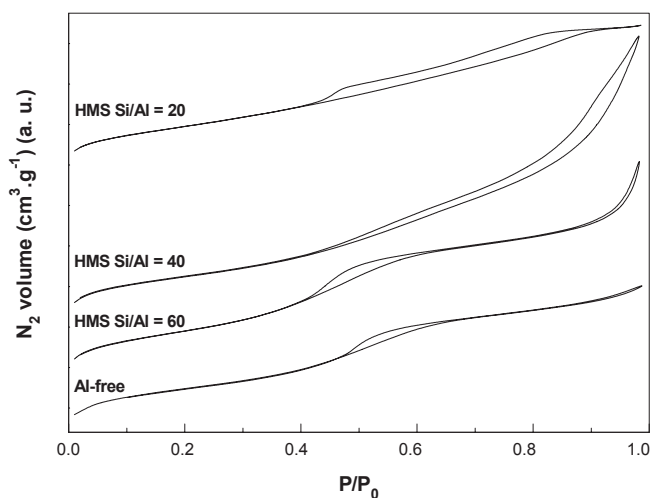**Fig. 2.** N_2 adsorption–desorption isotherms at −196 °C for the oxide catalyst precursors.

Table 1
Textural properties of the calcined catalysts and Al-modified supports as determined by N_2 adsorption–desorption isotherms at −196 °C.

Catalyst	S_{BET} (m²/g)
Al-free	544
HMS Si/Al = 60	517
HMS Si/Al = 40	451
HMS Si/Al = 20	483

support with a Si/Al = 40 ratio (451 m²/g). Table 1 shows the influence of Al loading on the specific S_{BET} values of the oxide catalyst precursors suggesting a partial blockage of the pores by the oxide species formed by the heteroatom [23].

On the other hand, NiMoW catalysts supported on Al free (HMS) and HMS with a Si/Al = 60 ratio, show the highest S_{BET} value among the catalysts studied. The lowest S_{BET} value was recorded for the catalysts containing a moderate Al-loading (Si/Al = 40). This result suggests that Ni–Mo-W species might be located not only inside the pores, but also an important fraction was probably located at the entrance of the mesopores [23]. The specific surface area of the Si/Al = 20 sample is higher than Si/Al = 40 sample. This effect can be related with a major segregation of the species (see XRD section) blocking the pores of support.

The pore size distributions of the HMS-Al (40) pure support and calcined NiMoW/HMS-Al(40) catalyst precursors calculated from the adsorption branch of the N_2 isotherm by using the Barret-Joyner-Halenda model are shown in Fig. 3. As seen in this figure, both samples show a uniform, narrow pore size distribution centred at 3.2 nm. The chemical and textural properties of the Al-HMS(40) and NiMoW/Al-HMS (40) samples are given in Table 2.

A comparison of the specific surface area values of the pure support and calcined catalyst indicates that S_{BET} decreases upon the incorporation of metal oxides. Simultaneously, the total pore volume decreases after metal oxides incorporation during catalyst preparation. The possible explanation of this increase is that the introduction of metals to the support blocked the small pores, so the decrease in surface area occurs. The large loss of total pore volume after metal loadings suggest the loss of microporosity is probably due pores blocking by guest metal oxides. To confirm the location of guest phases, the normalized BET surface area (NS_{BET}) was calculated.

The normalized S_{BET} (NS_{BET}) was calculated from the equation:

$$NS_{BET} = S_{BET} \text{ of catalyst}/[(1-y) \times S_{BET} \text{ of support}] \tag{2}$$

Fig. 1. Nitrogen adsorption–desorption isotherms of pure HMS-Al (40) support and calcined NiMoW/HMS-Al(40) catalyst.
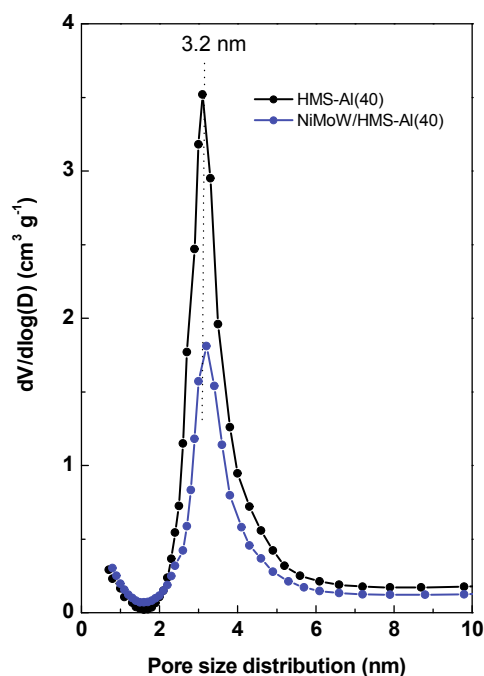
Fig. 3. Pore size distribution of the pure HMS-Al(40) support and calcined NiMoW/HMS-Al(40) catalyst as determined from adsorption branch of the N₂ adsorption data using the BJH method.

Table 2
Chemical[a] and textural properties[b] of Al-HMS (40) and NiMoW/Al-HMS (40) catalysts.

Support/ Catalyst	Ni (wt. %)	Mo (wt. %)	W (wt. %)	S_{BET} (m² g⁻¹)	NS_{BET}	V_{total} (cm³ g⁻¹)	d (nm)
NiMoW/Al-HMS(40)	3.8	7.1	8.7	451	0.88	0.77	4.7
Al-HMS (40)	–	–	–	689	–	1.30	5.0

[a] As determined by EDX/TEM analysis.
[b] As determined from N₂ adsorption–desorption isotherms at −196 °C for oxide precursors: S_{BET}: BET surface area (m²/$g_{support}$); V_{total}: total pore volume; d: average pore diameter (nm) calculated from adsorption data by BJH method

where y is the nominal metals content (wt%).

The NS_{BET} value close to 0.9 suggests the bimodal location of the metal oxides: on the external surface and within the inner porous structure (larger part).

3.1.2. X-ray diffraction (XRD)

Samples were analyzed by this characterization technique with the objective of studying the phases present in the synthesized materials. The low-angle X-ray patterns of the NiMoW/Al-HMS oxide precursors are shown in Fig. 4. As seen in this figure, all materials shows an intense single *d*100 reflection accompanied by more or less pronunciated diffuse scaterring centered at 0.65°, which indicates hexagonal symmetry. Higher order Bragg reflections are not resolved in the patterns of this material. However, it was demonstrated that similar "single-reflection" materials can still exhibit local hexagonal symmetry, as observed by selected area electron diffraction and TEM [32].

Fig. 5 shows the diffractograms of NiMoW catalysts supported on pure and modified HMS varying the aluminum content. All catalysts present a broad peak at approximately 2θ = 24° (diffraction angle), which is typical of amorphous silica [1]. On the other hand, reflections on the pattern belonging to the MoNiO₄ phase (JCDPS 00–008-0357)
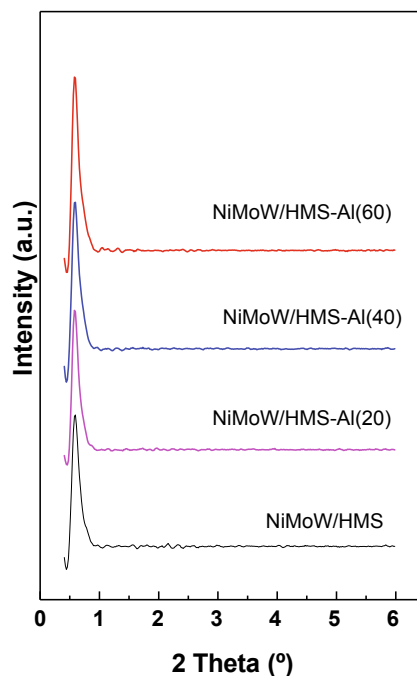

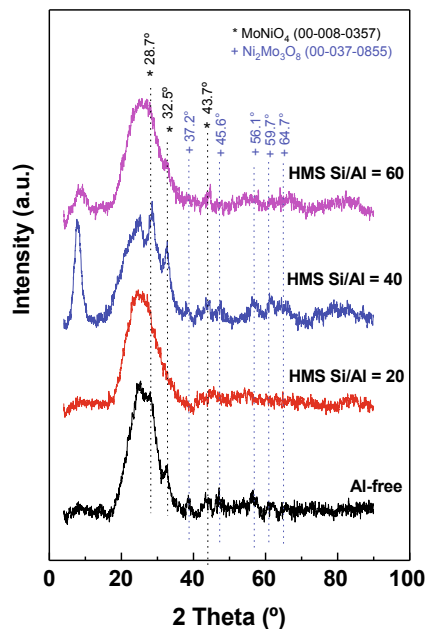**Fig. 4.** Low-angle XRD patterns of oxide precursors.

Fig. 5. X-ray diffractograms for the oxide catalysts precursors.

can be clearly seen in the angles of 28.7°, 32.5°, and 43.7° respectively, regardless the type of support. In addition Ni₂Mo₃O₈ phase (JCDPS 00-037-0855) was detected. It is possible that another type of crystalline phase was formed, however, if the crystal size of the present species is less than 5 nm, it is not possible to detect them by means of this technique.

3.1.3. UV–vis diffuse reflectance spectroscopy (DRS)

The coordination environment of Ni²⁺ and Mo⁶⁺ (W⁶⁺) ions in the precursors was studied by UV–vis diffuse reflectance spectroscopy (DRS-UV–vis). The UV–vis DRS spectra of the catalysts are shown in Fig. 6 as a Kubelka-Munk-Schuster function. Independently of the incorporation of
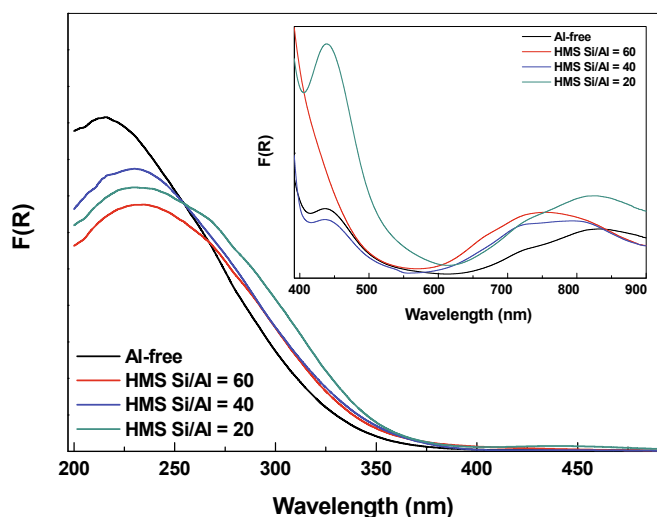
Fig. 6. DR UV–Vis spectra of the oxide catalysts precursors.

aluminum in the catalysts, they present two bands near 240 nm and 320 nm. The first involves the presence of ligand–metal charge transfer, which involves isolated transition metal sites attached to tungsten in tetrahedral coordination [33]. The shift in the bands mentioned could be attributed to the influence of tungsten on the electronic properties of this type of catalysts. A decrease of this type of species is observed in the case of the NiMoW catalysts supported on the HMS material with Si/Al ratio of 40. The tetrahedral species are more difficult to reduce and therefore to sulfide. The second band is assigned in literature to the transition ligand–metal charge O_2-Mo^{6+} (W^{6+}) from molybdenum and tungsten ions in octahedral coordination [34]. Additionally, DR UV–vis spectra exhibit bands in the 600–900 nm region. A "shoulder" is observed at 650 nm which could be related to Ni^{2+} ions coordinated in tetrahedral form. On the other hand, the band at 750 nm has been related to octahedral type Ni^{2+} ions [35].

As reported previously by us [28], by using Nuclear magnetic resonance, ^{27}Al NMR spectra for NiMoW/Al-HMS indicate that a larger amount of Al is incorporated into the framework of the HMS than in extraframework positions.

3.1.4. Desorption with ammonia at programmed temperature (TPD-NH$_3$)

The effect of modification of inorganic HMS support with Al (Si/Al = 20, 40 and 60) on the acidity was determined by TPD of NH_3 technique. Fig. 7, compares the TPD profiles of NH_3 of the precursors.
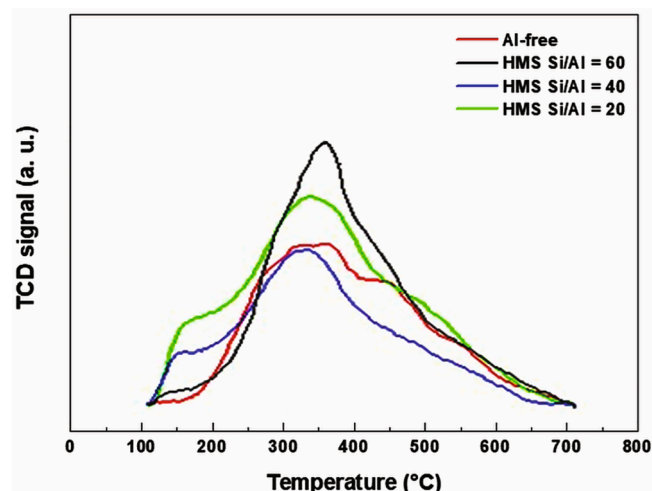

Fig. 7. TPD-NH$_3$ profiles for the oxide precursors.

The strength for the acid sites can be determined by using the temperature at which the ammonia molecule desorbs. Based on the desorption temperature, the acid sites were classified as weak (100–250 °C), medium (250–450 °C) or strong (T > 450 °C). All catalysts show weak, medium and strong acid sites. The first two peaks are attributed to weak Brønsted acid sites (Tmax ≈ 200 °C) and moderate (Tmax ≈ 300 °C), respectively. The concentration of acid sites expressed as mmol of desorbed NH_3 per gram of support is reported in Table 3.

As shown in this table, the total acidity shows the following trend: HMS Si/Al = 20 > HMS Si/Al = 60 > HMS Al- free > HMS Si/Al = 40. The total acidity could be related to the catalytic activity shown by the system investigated in this work. It was observed that the materials with lower acidity present higher overall rate values in the HDS reaction of DBT. Similarly, as the total acidity increased, there was a decrease in the catalytic activity (such as in the catalysts with Si/Al ratio of 20 and 60). It would be expected that as the aluminum ratio increases in the HMS structure, the acidity will increase; however, there is apparently no tendency for the acid sites with the Si/Al ratio of each material. This may be due to the modification of the structure of the support when impregnated with the active phase. It is important to mention that the active phase has an irregular dispersion on the surface of the support as shown in the TEM micrographs and this also causes molybdenum sulfide to modify the total acidity depending on the arrangement and stacking of the Mo(W)S$_2$ layers. As previously reported [36], a largest amount of Brønsted acid sites are formed by substitution of Si^{4+} ions by Al^{3+} ions during direct synthesis of the SBA-16-Al support. In this sense, one can expect that this behavior could be followed by our Al-HMS modified samples. In addition, A. Olivas and T. Zepeda [37], found that the dispersion of the active species (sulfide species) was related to the acidity of the support, this result can be asociated with the different values of length and stacking as reported in TEM section.

3.2. Characterization of catalysts in their sulfided state

3.2.1. Transmission electron microscopy (TEM)

Catalysts were studied by transmission electron microscopy since the transition metal sulfides are the active phases for the HDS reaction. Regarding the morphology of the support, in the images of TEM, we can observe some distorted areas, collapsed and pores. It is well known that the phases of Mo(W)S$_2$ adopt a structure in the form of layers with Mo atoms located in a trigonal prismatic coordination. All catalysts show the typical fringes of MoS$_2$ crystals. The location of the Mo(W)S$_2$ sheets in the HMS and Al-HMS carriers is shown in Fig. 8a–d.

In Fig. 8(a–d) are compared their magnification Mo(W)S$_2$ sheets. For all catalysts, the arrangement of W(Mo)S$_2$ layers parallel to the substrate indicates the basal plane attachment. No edge-plane attachment was observed because such species easily escape detection. The NiMoW/Al-HMS (40) sample show slightly higher W(Mo)S$_2$ slabs density than their counterparts. In addition, there is a slight increase on the stacking density of Mo(W)S$_2$ for the catalysts supported on pure HMS and HMS with Si/Al ratio of 40, than their counterparts HMS samples with Si/Al ratio of 60 and 20. A higher density of Mo(W)S$_2$ in the catalysts could affect the catalytic activity in the HDS of DBT. The distribution of the stacking length and number of stripes is shown in Table 4, respectively. Data showed larger particles that are formed on the HMS catalysts with Si/Al ratio of 60 (Fig. 8d). The interplanar distance of the (002) planes of

Table 3
Acidities of the oxide precursors (from TPD-NH$_3$).

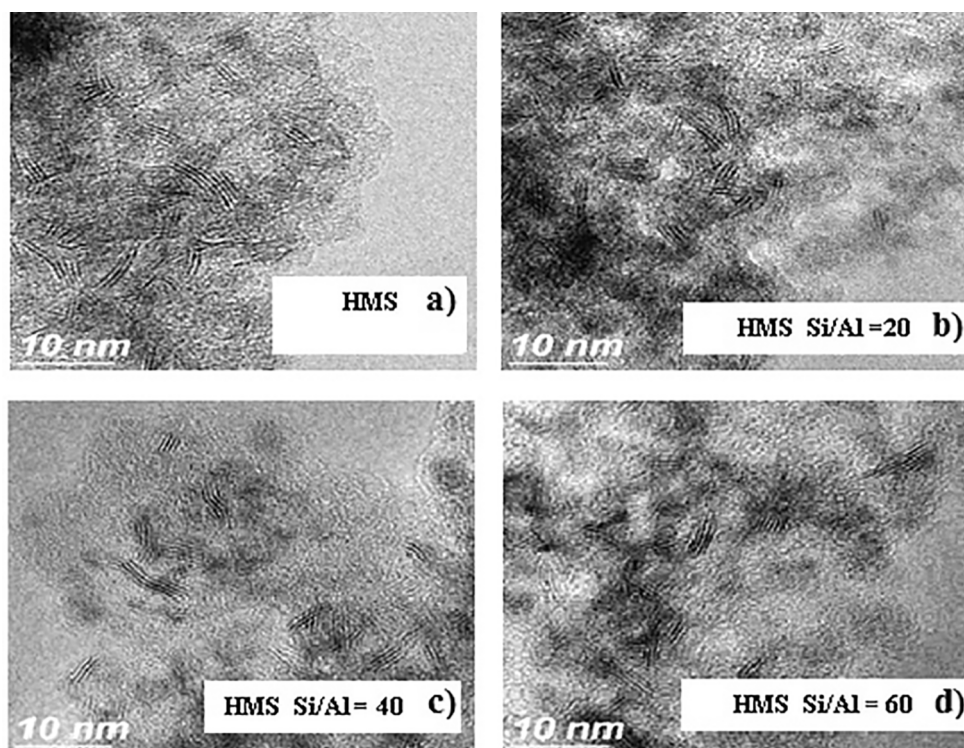| Catalyst	Amount of acid sites (mmol NH$_3$/g)			
	Weak	Medium	Strong	Total
Al-free	1.2	1.1	1.0	3.3
HMS Si/Al = 60	0.0	3.5	0.5	4.0
HMS Si/Al = 40	0.3	1.8	0.8	2.9
HMS Si/Al = 20	0.3	3.4	0.7	4.4

Fig. 8. TEM images of the fresh sulfided catalysts.

Table 4
Summary of the MoS$_2$ crystal sizes determined by HRTEM.

Catalyst	Layer length (nm) ($\pm$1.8)	Stacking layers ($\pm$1)
Al-free	6.4	2.2
HMS Si/Al = 60	7.1	2.4
HMS Si/Al = 40	6.4	2.5
HMS Si/Al = 20	4.7	1.3

all catalysts was very similar (0.67 nm) and slightly higher than those of the pure MoS$_2$ (0.616 nm) and WS$_2$ phase (0.618 nm). This could be indicative that Al atoms were located along the (002) direction into the crystalline structure of Mo(W)S$_2$ or may be caused by the stress released by curved fringes, the dislocation of the coplanarity of the MoS$_2$ planes by organic molecules or due to the synergistic effect resulting from the intercalation of Ni atoms into the interlayer space of MoS$_2$ crystallites [38–40]. More information on the morphology of phases formed can be revealed by statistical evaluation of about 50 particles from various TEM images.

3.2.2. X-ray diffraction (XRD)

Fig. 9a–d shows the X-ray diffractograms of sulfided catalysts supported on inorganic pure HMS and modified with aluminum. In these patterns the typical planes (002), (100), (103), (105) and (110) are observed with signals at 14, 33, 40, 50 and 58° 2θ (2θ = x "diffraction angle"), respectively corresponding to both poorly crystalline 2H-MoS$_2$ and WS$_2$ structures (JCPDS-ICDD 8–237, 37–1492). When aluminum is incorporated on the support, the intensity of the peak (002) is increased, mainly for the catalyst supported on HMS with Si/Al ratio of 40, which is related to a higher stacking of the Mo(W)S$_2$ in the direction of the axis "c".

In addition, it is observed the presence of a wide band approximately in 2θ = 24° characteristic of amorphous silica (SiO$_2$). The presence of nickel species is not clearly visible. The low intensity of these peaks indicates that the species supported may be well dispersed on the surface
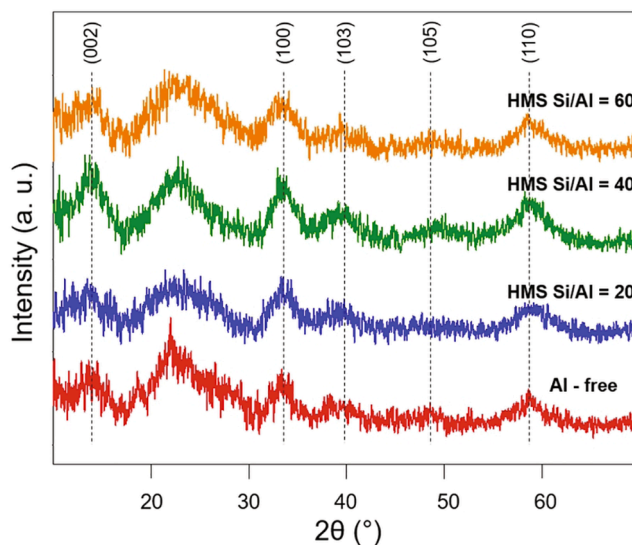

Fig. 9. X-ray diffractograms of the NiMoW sulfided catalysts.

of the supports.

3.3. Evaluation of catalytic properties (activity and selectivity) in the dibenzothiophene (DBT) hydrodesulfurization reaction (HDS)

The overall reaction rate and selectivity data at 30% DBT conversion are shown in Tables 5 and 6, respectively.

In according to the catalytic activity, the evaluated materials showed a good performance and a high activity in the HDS reaction of DBT, since the DBT conversion values were 97–99%. The following trend was observed with respect to the overall reaction rate in the HDS of DBT over the trimetallic samples: Al-free > HMS Si/Al = 40 > HMS Si/Al = 60 > HMS Si/Al = 20. It was observed that in the trimetallic catalysts, the

Table 5

Conversion results and overall rates of the catalysts used in the HDS of DBT. Reaction conditions: $T = 320\,°C$; $P = 5.4$ MPa; Reaction time $= 4.5$ h.

Catalyst	DBT Conversion %	Overall reaction rate $* 10^8$ $mol_{DBT}.(g_{CAT}.s)^{-1}$
Al-free	99	71.6
HMS Si/Al = 60	99	57.5
HMS Si/Al = 40	98	69.0
HMS Si/Al = 20	97	46.8

Table 6

Selectivity data at 30% DBT conversion for sulfided NiMoW/HMS and HMS-Al catalysts.

Selectivity at 30% conversion			
Catalyst	HYD	DDS	HYD/DDS
Al-free	26%	74%	0.35
HMS Si/Al = 60	30%	70%	0.42
HMS Si/Al = 40	34%	66%	0.51
HMS Si/Al = 20	23%	77%	0.29

incorporation of aluminum into the HMS framework decreases the catalytic activity. On the other hand, the addition of a moderate amount of aluminum (HMS Si/Al = 40 sample) produces a good performance in the HDS of the DBT reaction, compared to that shown by the HMS Si/Al = 60 and HMS Si/Al = 20 catalysts. A tendency between activity and acidity was observed in this work, since a decrease in the catalytic activity might be related with an increase of the total surface acidity. Materials with lower acidity present higher overall rate values in the HDS reaction of DBT. Likewise, as the total acidity increased, there was a decrease in the catalytic activity (HMS Si/Al = 20 and 60). However, the correlation of the catalyst activity with the acidity of oxide precursors is only a rough approximation and more investigation should be made to elucidate this since the HDS of DBT occurs mainly via DDS route which take place on the Ni-promoted metal sulfides by extracting an S-atom by hydrogenolysis [41]. In such a case, the catalyst acidity may help only to C—S bond cleavage by cracking. On the other hand, considering the work reported by A.P. Glotov et al. [42] and our catalytic activity results, one may expect that the interaction between the active species and the support surface should be increased when Al is incorporated in a higher amount, decreasing the reducibility and the catalytic activity, showing an optimum for NiMoW/Al-HMS (40) sample. In previous works, we found that addition of Al, Ti or Zr leads to a noticeable improvement during the performance of bimetallic catalysts (NiMo, CoMo, NiW). However, in this work we study a ternary system (NiMoW). The incorporation of Al increased the interaction between active species and the surface, decreasing the reducibility of the species. On the other hand, in a previous report [1] it was found that in a CoMoW trimetallic system, the species of tungsten can decorate the surface of molybdenum species resulting in a minor reducibility and catalytic activity.

In this study all catalysts showed preferential DBT transformation via direct desulfurization reaction route being hydrogenation route of DBT transformation strongly inhibited (Table 6).

The NiMoW/HMS (Si/Al = 60) catalyst shows a slightly increase in HYD compared with that reported for Al-free and a slightly higher DBT conversion value compared with that observed for the HMS (Si/Al = 40) sample. An improvement in hydrogenation activity due to accumulation of H_2S in a batch reactor was observed previously [43]. This could be explained assuming Kasztelan [44] model that the coordinatively unsaturated sites (CUS) and sulfur-saturated sites are responsible for hydrogenolysis (C—S bond scission) and hydrogenation, respectively, of DBT molecules on the MoS_2 (WS_2) active sites. Since it is well documented that the H_2S is adsorbed dissociatively on the coordinatively unsaturated (sulfur-vacancy) sites [45], the inhibition of the hydrogenolysis occur when H_2S formed is dissociatively adsorbed on the CUS

sites leading to formation of S-saturated sites. Besides, some enhancement of the catalyst HYD function may occur but the DDS reaction route remains as the main reaction route.

In the case of Al-free sample, the formation of "brim sites" is highly possible because this sample showed the formation of more "curved" Mo $(W)S_2$ phases. In this sense, Berhault and co-workers [46] observed that the bending of the MoS_2 slabs modifies the HDS properties of the sulfided $CoMo/Al_2O_3$ catalysts by creating active sites on curved layers of the MoS_2 phase. Moreover, the layers of MoS_2 phase formed by sulfidation of the irregular molybdenum oxide species might have a higher amount of coordinatively unsaturated sites (CUS) than those formed from regular MoO_3 phase. In addition, we found that the catalytic performance might be related to the dispersion and density of $Mo(W)S_2$ in the catalysts as observed in TEM.

Finally, with respect to the selectivity, a trend toward the direct desulfurization (DDS) path was observed: HMS Si/Al = 20 > Al-free > HMS Si/Al = 60 > HMS Si/Al = 40. This behavior could be related to the structure and morphology of the synthesized materials, since a very similar tendency is observed in the stacking of the $Mo(W)S_2$ measured by TEM.

4. Conclusions

The incorporation of aluminum into the inorganic HMS framework causes important changes in the structural, textural and physicochemical properties of the trimetallic NiMoW catalysts, synthesized by an incipient impregnation method. Regarding the structure, the presence of poorly crystalline phases of $Mo(W)S_2$ was observed, probably due to the type of precursor used in addition to the synthesis method, nonetheless an effect of aluminum incorporation is observed on the stacking of the $Mo(W)S_2$ layers. The catalytic activity could be related to the total acidity quantified by TPD of NH_3 for the system investigated in this work. This is because there is a tendency between acidity and the overall rate in the HDS reaction of DBT. Materials with lower acidity have higher overall rate values in the HDS reaction of DBT. On the other hand, when the total acidity was high, there was a decrease in the catalytic activity. In addition, we found that the catalytic performance might be related to the dispersion and density of $Mo(W)S_2$ in the catalysts.

Declaration of Competing Interest

The authors declare that they have no known competing financial interests or personal relationships that could have appeared to influence the work reported in this paper.

Acknowledgements

References

[1] R. Obeso-Estrella, J.L.G. Fierro, J.N. Díaz de León, S. Fuentes, G. Alonso-Nuñez, E. Lugo-Medina, B. Pawelec, T.A. Zepeda, Effect of partial Mo substitution by W on HDS activity using sulfide CoMoW/Al$_2$O$_3$–TiO$_2$ catalysts, Fuel 233 (2018) 644–657, https://doi.org/10.1016/j.fuel.2018.06.078.

[2] W. Zhoua, Q. Weib, Y. Zhoub, M. Liub, S. Dingb, Q. Yang, Hydrodesulfurization of 4,6- dimethyldibenzothiophene over NiMo sulfide catalysts supported on meso-microporous Y zeolite with different mesopore sizes, Appl. Catal. B. Environ. 238 (2018) 212–224, https://doi.org/10.1016/j.apcatb.2018.07.042.

[3] K. Kohli, R. Prajapati, S.K. Maity, M. Sau, B.K. Sharm, Accelerated pre-coking of NiMo/γ-Al$_2$O$_3$ catalyst: Effect on the hydroprocessing activity of vacuum residue, Fuel 235 (2019) 437–447, https://doi.org/10.1016/j.fuel.2018.08.026.

[4] M.S. Rana, A. Al-Barood, R. Brouresli, A.W. Al-Hendi, N. Mustafa, Effect of organic nitrogen compounds on deep hydrodesulfurization of middle distillate, Fuel Process. Technol. 177 (2018) 170–178, https://doi.org/10.1016/j.fuproc.2018.04.014.

[5] A. Stanislaus, A. Marafi, M.S. Rana, Recent advances in the science and technology of ultra low sulfur diesel (ULSD) production, Catal. Today 153 (1-2) (2010) 1–68, https://doi.org/10.1016/j.cattod.2010.05.011.

[6] S.Y. Gómez-Orozco, R. Huirache-Acuña, B. Pawelec, J.L.G. Fierro, E.M. Rivera-Muñoz, J. Lara-Romero, G. Alonso-Nuñez, Characterizations and HDS performances of sulfided NiMoW catalysts supported on mesoporous titania-modified SBA-15, Catal. Today 305 (2018) 152–161, https://doi.org/10.1016/j.cattod.2017.08.009.

[7] J.C. García-Martínez, H.A. González Uribe, M.M. González-Brambila, J.A. Colín-Luna, Y.E. Escobedo-García, A. López-Gaona, L. Alvarado-Perea, Selective adsorption of nitrogen compounds using silica-based mesoporous materials as a pretreatment for deep hydrodesulfurization, Catal. Today 305 (2018) 40–48, https://doi.org/10.1016/j.cattod.2017.10.037.

[8] T.T. Nguyen, E.W. Qian, Synthesis of mesoporous Ti-inserted SBA-15 and CoMo/Ti-SBA-15 catalyst for hydrodesulfurization and hydrodearomatization, Microporous Mesoporous Mater 265 (2018) 1–7, https://doi.org/10.1016/j.micromeso.2018.01.026.

[9] T. Chiranjeevi, P. Kumar, M.S. Rana, G. Murali Dhar, T.S.R. Prasada Rao, Physico-chemical characterization and catalysis on mesoporous Al-HMS supported molybdenum hydrotreating catalysts, J. Mol. Catal. A Chem. 181 (1–2) (2002) 109–117, https://doi.org/10.1016/S1381-1169(01)00352-1.

[10] T. Chiranjeevi, P. Kumar, S.K. Maity, M.S. Rana, G. Murali Dhar, T.S.R. Prasada Rao, Characterization and hydrodesulfurization catalysis on WS2 supported on mesoporous Al–HMS material, Micropor. Mesopor. Mater. 44–45 (2001) 547–556, https://doi.org/10.1016/S1387-1811(01)00233-5.

[11] A.V. Vutolkina, A.P. Glotov, A.V. Zanina, D.F. Makhmutov, A.L. Maximov, S.V. Egazar'yants, E.A. Karakhanov, Mesoporous Al-HMS, and Al-MCM-41 supported Ni- Mo sulfide catalysts for HYD and HDS via in situ hydrogen generation through a WGSR, Catal. Today 329 (2019) 156–166, https://doi.org/10.1016/j.cattod.2018.11.030.

[12] R. Palcheva, L. Kaluz, L. Dimitrov, G. Tyuliev, G. Avdeev, K. Jirátová, A. Spojakin, NiMo catalysts supported on the Nb modified mesoporous SBA-15 and HMS: Effect of thioglycolic acid addition on HDS, Appl. Catal. A. Gen. 520 (2016) 24–34, https://doi.org/10.1016/j.apcata.2016.04.008.

[13] P.J. Vázquez-Salas, R. Huirache-Acuña, T.A. Zepeda, G. Alonso-Núñez, R. Maya-Yescas, N. Mota, B. Pawelec, Enhancement of dibenzothiophene hydrosulphurization via hydrogenation route on NiMoW catalyst supported on HMS modified with Ti, Catal. Today 305 (2018) 65–74, https://doi.org/10.1016/j.cattod.2017.10.005.

[14] G. Muthu Kumaran, S. Garg, K. Soni, L.D. Manoj Kumar, G.M. Sharma, K.S.R. Dhar, Rao, Effect of Al-SBA-15 support on catalytic functionalities of hydrotreating catalysts I. Effect of variation of Si/Al ratio on catalytic functionalities, Appl. Catal. A: General 305 (2019) 123–129, https://doi.org/10.1016/j.apcata.2006.02.057.

[15] J.A. Mendoza-Nieto, A. Vizueth-Montes de Oca, L.A. Calzada, T.E. Klimova, Trimetallic NiMoW and CoMoW catalysts supported on SBA-15 modified with titania or zirconia for deep hydrodesulfurization, Catal. Today, (2019) doi.org/10.1016/j.cattod.2019.06.023.

[16] V.A. Valles, Y. Sangasaeng, M.L. Martínez, S. Jongpatiwut, A.R. Beltramone, HDT of the model diesel feed over Ir-modified Zr-SBA-15 catalysts, Fuel 240 (2019) 138–152, https://doi.org/10.1016/j.fuel.2018.11.148.

[17] J.C. Morales-Ortuño, T.E. Klimova, Development of new hydrodesulfurization NiMo catalysts supported on Al2O3-TiSBA-15 hybrid materials, Fuel 198 (2017) 99–109, https://doi.org/10.1016/j.fuel.2017.01.007.

[18] T. Halachev, J.A. de los Reyes, C. Araujo, L. Dimitrov, G. Cordoba, Hydrodesulfurization of dibenzothiophene over Ni-Mo/(P)Ti-HMS catalysts, Stud. Surf. Sci. Catal. 127 (1999) 401–404, https://doi.org/10.1016/S0167-2991(99)80440-6.

[19] A. Kokliukhin, M. Nikulshina, A. Sheldaisov-Meshcheryakov, A. Mozhaev, P. Nikulshin, CoMo Hydrotreating Catalysts Supported on Al2O3, SiO2 and SBA-15 Prepared from Single Co2Mo10-Heteropolyacid. In Search of Self-Promotion Effect, Catal. Lett. 148 (9) (2018) 2869–2879, https://doi.org/10.1007/s10562-018-2480-7.

[20] A.S. Koklyukhin, M.S. Nikul'shina, A.A. Sheldaisov-Meshcheryakov, A.V. Mozhaev, C. Lancelot, P. Blanchard, C. Lamonier, P.A. Nikul'shin, Activity of Mo(W)S2/SBA-15 Catalysts Synthesized from SiMoW Heteropoly Acids in 4,6-Dimethyldibenzo-thiophene Hydrodesulfurization, Pet. Chem. 59 (12) (2019) 1293–1299, https://doi.org/10.1134/S0965544119120077.

[21] M.S. Nikulshina, A.V. Mozhaev, A.A. Sheldaisov-Meshcheryakov, P.A. Nikulshin, Mono- and Bimetallic Mo(W)S2/Al2O3 and Mo(W)S2/SBA-15 Hydrotreating Catalysts Based on SiMo12 and SiW12 Heteropoly Acids, Pet. Chem. 57 (12) (2017) 1058–1064, https://doi.org/10.1134/S0965544117120118.

[22] E.R. Naranov, O.V. Golubev, A.I. Guseva, P.A. Nikulshin, A.L. Maksimov, E.A. Karakhanov, Hydrotreating of middle-distillate fraction on sulfide catalysts containing crystalline porous aluminosilicates, Pet. Chem. 57 (12) (2017) 1151–1155, https://doi.org/10.1134/S0965544117060226.

[23] T.A. Zepeda, Comparison and performance of different sulphided Ti-loaded mesostructured silica-supported CoMo catalysts in deep HDS, Appl. Catal. A: Gen. 347 (2) (2008) 148–161, https://doi.org/10.1016/j.apcata.2008.06.012.

[24] C. Thomazeau, C. Geantet, M. Lacroix, M. Danot, V. Harlé, P. Raybaud, Predictive approach for the design of improved HDT catalysts: γ-Alumina supported (Ni, Co) promoted Mo1−xWxS2 active phases, Appl. Catal. A: Gen. 322 (2007) 92–97, https://doi.org/10.1016/j.apcata.2007.01.016.

[25] A.V. Vutolkina, D.F. Makhmutov, A.V. Zanina, A.L. Maximov, D.S. Kopitsin, A.P. Glotov, S.V. Egazar'yants, E.A. Karakhanov, Hydroconversion of thiophene derivatives over dispersed Ni–Mo Sulfide Catalysts, Pet. Chem. 58 (14) (2018) 1227–1232, https://doi.org/10.1134/S0965544118140141.

[26] M.I. Knyazeva, D.I. Panyukova, A.L. Maximov, Properties of nanosized cobalt-molybdenum sulfide catalyst formed in situ from sulfonium thiosalt, Pet. Chem. 59 (2019) 504–510, https://doi.org/10.1134/S0965544119050049.

[27] S.L. Soled, S. Miseo, R. Krycak, H. Vroman, T.C. Ho, K. Riley, Nickel Molybdotungstate Hydrotreating Catalysts, United States Patent 6,299,760 October 9, (2001).

[28] R. Huirache-Acuña, B. Pawelec, C.V. Loricera, E.M. Rivera-Muñoz, R. Nava, B. Torres, J.L.G. Fierro, Comparison of the morphology and HDS activity of ternary Ni(Co)-Mo-W catalysts supported on Al-HMS and Al-SBA-16 substrates, Appl. Catal. B: Environ. 125 (2012) 473–485, https://doi.org/10.1016/j.apcatb.2012.05.034.

[29] S. Zulkepli, J.C. Juan, H.V. Lee, N.S. Abd Rahman, P. Loke Show, E. Poh Ng, Modified mesoporous HMS supported Ni for deoxygenation of triolein into hydrocarbon-biofuel production, Energ. Convers. and Manege. 165 (2018) 495–508, https://doi.org/10.1016/j.enconman.2018.03.087.

[30] Y. Sakamoto, M. Kaneda, O. Terasaki, D.Y. Zhao, J.M. Kim, G. Stucky, H.J. Shin, R. Ryoo, Direct imaging of the pores and cages of three-dimensional mesoporous materials, Nature 408 (6811) (2000) 449–453, https://doi.org/10.1038/35044040.

[31] M. Muttakin, S. Mitra, K. Thu, K. Ito, B. Baran Saha, Theoretical framework to evaluate minimum desorption temperature for IUPAC classified adsorption isotherms, Int. J. Heat Mass Transfer 122 (2018) 795–805, https://doi.org/10.1016/j.ijheatmasstransfer.2018.01.107.

[32] P.T. Tanev, M. Chibwe, T.J. Pinnavaia, Titanium-containing mesoporous molecular sieves for catalytic oxidation of aromatic compounds, Nature 368 (6469) (1994) 321–323, https://doi.org/10.1038/368321a0.

[33] J.G. Graselli, B.J. Bulkin, Analytical Raman Spectroscopy, Wiley, New Cork, 1991, p. 352.

[34] R.A. Schoonheydt, Diffuse reflectance spectroscopy, in: F. Delannay (Ed.), Characterization of Heterogeneous Catalysts, Marcel Dekker, New York, 1984, p. 125.

[35] P. Atanasova, T. Halachev, J. Uchytil, M. Kraus, Effect of phosphorus on the surface concentration of molybdenum and nickel in the oxide form of nickel-molybdenum/alumina catalysts and on their hydrodesulphurization activity, Appl. Catal. A: Gen. 38 (2) (1988) 235–240, https://doi.org/10.1016/S0166-9834(00)82828-6.

[36] R. Huirache-Acuña, T.A. Zepeda, E.M. Rivera-Muñoz, R. Nava, C.V. Loricera, B, Pawelec Characterization and HDS performance of sulfide CoMoW catalysts supported on mesoporous Al-SBA-16 substrates, Fuel 149 (2015) 149–161, https://doi.org/10.1016/j.fuel.2014.08.045.

[37] A. Olivas, T.A. Zepeda, Impact of Al and Ti ions on the dispersion and performance of supported NiMo(W)/SBA-15 catalysts in the HDS and HYD reactions, Catal. Today 143 (1-2) (2009) 120–125, https://doi.org/10.1016/j.cattod.2008.09.001.

[38] J.V. Lauritsen, J. Kibsgaard, G.H. Olesen, P.G. Moses, B. Hinneman, S. Helveg, J.K. Nørskov, B.S. Clausen, H. Topsøe, E. Lægsgaard, F. Besenbacher, Location and coordination of promoter atoms in Co- and Ni-promoted MoS2-based hydrotreating catalysts, J. Catal. 249 (2007) 220–233, https://doi.org/10.1016/j.jcat.2007.04.013.

[39] B.S. Zhang, Y.J. Yi, W. Zhang, C.H. Liang, D.S. Su, Electron microscopy investigation of the microstructure of unsupported Ni-Mo-W Sulfide, Mater. Charact. 62 (7) (2011) 684–690, https://doi.org/10.1016/j.matchar.2011.04.022.

[40] P. Afanasiev, Topotactic of size-tuned MoS2 inorganic fullerenes that allows revealing particular catalytic properties of curved basal planes, Appl. Catal. B: Environ. 227 (2018) 44–53, https://doi.org/10.1016/j.apcatb.2017.12.012.

[41] J.J. Lee, H. Kim, S.H. Moon, Preparation of highly loaded, dispersed MoS2/Al2O3 catalysts for the deep hydrodesulfurization of dibenzothiophenes, Appl. Catal. B. Environ. 41 (1-2) (2003) 171–180, https://doi.org/10.1016/S0926-3373(02)00209-6.

[42] A.P. Glotov, A.V. Vutolkina, N.A. Vinogradov, A.A. Pimerzin, V.A. Vinokurov, Al.A. Pimerzin, Enhanced HDS and HYD activity of sulfide Co-PMo catalyst supported on alumina and structured mesoporous silica composite. Catal. Today In Press 2020. https://doi.org/10.1016/j.cattod.2020.10.010.

[43] M.S. Rana, R. Navarro, J. Leglise, Competitive effects of nitrogen and sulfur content on activity of hydrotreating CoMo/Al2O3 catalysts: a batch reactor study, Catal. Today 98 (1-2) (2004) 67–74, https://doi.org/10.1016/j.cattod.2004.07.020.

[44] S. Kasztelan, A descriptive model of surface sites on MoS2 (WS2) particles, Langmuir 1990, 6, 690-595. https://doi.org/10.1021/la00093a013.

[45] M. Echard, J. Leglise, Sulfidation of an oxidic CoMo/Al2O3 catalyst under practical conditi ons: different kinds of sulfur species, Catal. Lett. 72 (1–2) (2001) 83–89, https://doi.org/10.1023/A:1009037211108.

[46] A. Nogueira, R. Znaiguia, D. Uzio, P. Afanasiev, G. Berhault, Curved nanostructures of unsupported and Al2O3-supported MoS2 catalysts: Synthesis and HDS catalytic properties, Appl. Catal. A. Gen. 429-430 (2012) 92–105, https://doi.org/10.1016/j.apcata.2012.04.013.